PHYSICAL REVIEW B VOLUME 5, NUMBER 8 15 APRIL 1972

Elastic Moduli and Phonon Properties of Bi_2Te_3 †

J. O. Jenkins
Bell Telephone Laboratories, Naperville, Illinois 60540
and
J. A. Rayne
Carnegie-Mellon University, Pittsburgh, Pennsylvania 15213
and
R. W. Ure, Jr.
University of Utah, Salt Lake City, Utah 84112
(Received 7 January 1972)

The six independent elastic moduli of Bi_2Te_3 have been measured from 4.2 to 300 K using a continuous-wave resonance technique. Extrapolation of the measurements to absolute zero gives $C_{11}=7.436$, $C_{66}=2.619$, $C_{33}=5.160$, $C_{44}=3.135$, $C_{13}=2.917$, and $C_{14}=1.541$ in units of 10^{11} dyn/cm^2. These values correspond to a limiting Debye temperature of 164.9 ± 0.2 K, which agrees with the calorimetric value of 165 ± 2 K. A Born–von Kármán lattice model providing for central and angular forces between first and second neighbors is constructed to fit the moduli. Using the model, the frequencies of infrared absorption and Raman scattering are predicted and the density of phonon states and lattice specific heat are found. The calculated specific heat differs appreciably from the calorimetric measurements, indicating the possible importance of third- and fourth-neighbor interactions.

I. INTRODUCTION

There has recently been considerable interest in the phonon spectrum of bismuth telluride. Specific-heat data[1] show that the validity of the Debye model does not extend above 1 K, presumably as a result of the weak bonding between the cleavage planes existing in the material. Furthermore, transport measurements[2] have shown the importance of anisotropic phonon-electron scattering in determining the magnetoresistance coefficients. Both sets of experiments indicate the importance of establishing the lattice properties of bismuth telluride in considerable detail.

Information about the phonon spectrum may, of course, be found directly from inelastic neutron scattering as well as from infrared and Raman scattering experiments. Since these data are not as yet available, the present study of the elastic moduli has been undertaken. From a fit of the data to a Born–von Kármán lattice model, the phonon dispersion relations and the lattice specific heat have been calculated. The fit of the latter to experiment is not good and indicates that the interatomic forces probably involve third and fourth nearest neighbors, as in the case of bismuth.[3]

II. EXPERIMENT

A. Crystal Structure and Properties of Bi_2Te_3

The unit cell for the Be_2Te_3 structure is rhombohedral and contains the five atoms in one molecule. At 293 K the rhombohedral unit-cell parameters are[4]

$$a_R = 10.473\ \text{Å}, \quad \alpha_R = 24.159^\circ ,$$

which correspond to the hexagonal unit-cell dimensions

$$a = 4.3835\pm0.0005\ \text{Å}, \quad c = 30.487\pm0.001\ \text{Å} .$$

The density calculated from these parameters and the molecular weight is 7.8624 g/cm^3.

Bi_2Te_3 belongs to the space group $R\bar{3}m$, which has the following principal symmetry operations: a threefold-rotation (trigonal) axis, three twofold-rotation (binary) axes perpendicular to the trigonal axis, three mirror planes perpendicular to the binary axes, and an inversion center. For convenience in performing the lattice dynamical calculation and to define uniquely the components of the elastic modulus tensor, it is necessary to give a complete specification of the Cartesian reference axes in terms of the rhombohedral axes. The z axis is chosen along the trigonal axis in the [111] rhombohedral direction, the y axis is chosen in a mirror plane in the $[\bar{1}\,\bar{1}\,2]$ direction along the positive projection of a basis vector, and the x axis, completing the right-handed system, lies along the binary axis in the $[\bar{1}10]$ direction. Correspondingly, the Cartesian components of the rhombohedral basis vectors are

$$\begin{aligned}
\vec{a}_1 &= -\tfrac{1}{2}a\,\vec{i} - \tfrac{1}{6}\sqrt{3}a\,\vec{j} + \tfrac{1}{3}c\,\vec{k} ,\\
\vec{a}_2 &= \tfrac{1}{2}a\,\vec{i} - \tfrac{1}{6}\sqrt{3}a\,\vec{j} + \tfrac{1}{3}c\,\vec{k} ,\\
\vec{a}_3 &= \tfrac{1}{3}\sqrt{3}a\,\vec{j} + \tfrac{1}{3}c\,\vec{k} .
\end{aligned} \tag{1}$$

The sign of the elastic modulus c_{14} depends on the

choice of Cartesian axes. Our choice agrees with that of Eckstein *et al.*[5] and Epstein *et al.*[6] in their work on bismuth and antimony, respectively, but it disagrees with that given by Drabble in his review of the properties of Bi_2Te_3.[7]

To identify each atom and represent its position in the structure, the usual notation is used:

$$\vec{x}(\vec{t}; s) = t_1\vec{a}_1 + t_2\vec{a}_2 + t_3\vec{a}_3 + \vec{r}_s , \qquad (2)$$

where $\vec{t}$ refers to the position of the unit cell in terms of the basis vectors, and $\vec{r}_s$ is the position of the sth atom in the basis relative to the origin of the cell. The five atoms in the basis for Bi_2Te_3 lie along the trigonal axis at the fractional positions $(0, \pm v)$ for the tellurium atoms and $\pm u$ for the bismuth atoms. The quantities u and v have been determined[8] at 293 K to be 0.4001 and 0.2095. There are two inequivalent lattice sites for Te designated by the subscripts 1 and 2, with the Te_2 atom lying at the inversion center. A portion of the Bi_2Te_3 lattice is shown in Fig. 1, with the $(\vec{t}; s)$ notation, including the five atoms in the zero unit cell and the twelve closest neighbors of each. It is evident from the figure that there are planes of equivalent atoms perpendicular to the trigonal axis in the order

$$- Te_1 - Te_1 - Bi - Te_2 - Bi - Te_1\text{-}Te_1\text{-}Bi- \cdot$$

It is found that Bi_2Te_3 cleaves very easily perpendicular to the trigonal axis and this property is attributed to a weak, van der Waals bond between the adjacent Te_1 layers. This weak bond may be expected to cause some simplification in the lattice dynamics. The remaining physical properties are discussed at length in the review by Drabble.[7]

B. Ultrasonic Measurements of Elastic Moduli

In this section the crystal is treated as a linear, continuous medium characterized by a matrix of elastic moduli. The most general matrix C_{ij} allowed for a medium of $\bar{3}m$ symmetry, such as Bi_2Te_3, is[9]

$$C_{ij} = \begin{pmatrix} C_{11} & C_{12} & C_{13} & C_{14} & 0 & 0 \\ C_{12} & C_{11} & C_{13} & -C_{14} & 0 & 0 \\ C_{13} & C_{13} & C_{33} & 0 & 0 & 0 \\ C_{14} & -C_{14} & 0 & C_{44} & 0 & 0 \\ 0 & 0 & 0 & 0 & C_{44} & C_{14} \\ 0 & 0 & 0 & 0 & 0 & C_{66} \end{pmatrix} , \qquad (3)$$

where $C_{12} = C_{11} - 2C_{66}$. Thus there are six independent moduli, namely, C_{11}, C_{66}, C_{33}, C_{44}, C_{13}, and C_{14}, to be determined.

The usual ultrasonic methods[10] of determining the elastic moduli involve the measurement of the phase velocity of plane waves in a sample having

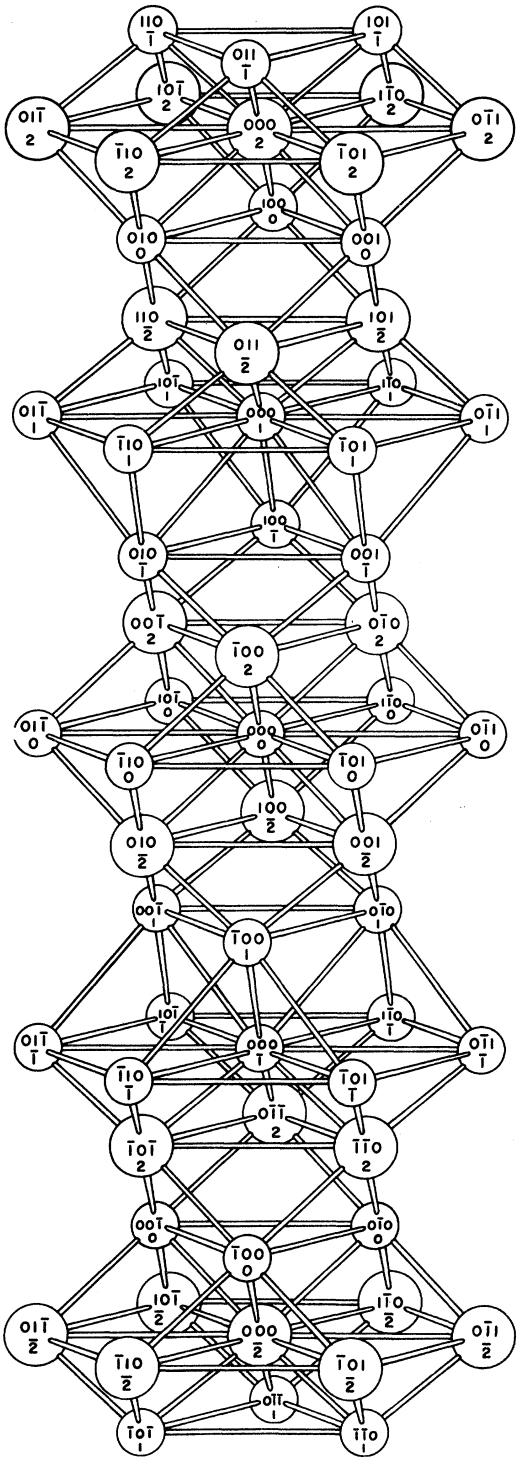

FIG. 1. Representation of the crystal structure of Bi_2Te_3 showing the hexagonal unit cell. Tellurium and bismuth atoms, designated by the smaller and larger circles, respectively, are indexed according to the scheme explained in the text. No physical significance is to be attached to the lines joining the atoms.

TABLE I. Propagation modes for ultrasonic velocity measurements in crystal of $R\bar{3}m$ symmetry.

Mode number	Axis	Effective modulus	Propagation vector	Polarization vector
1	x	C_{11}	[1,0,0]	[1,0,0]
2		C_{x+}		$[0, C_{14}, C_{x+} - C_{66}]$
3		C_{x-}		$[0, C_{14}, C_{x-} - C_{66}]$
5	y	C_{66}	[0,1,0]	[1,0,0]
4		C_{y+}		$[0, C_{14}, C_{11} - C_{y+}]$
6		C_{y-}		$[0, C_{14}, C_{11} - C_{y-}]$
7	z	C_{33}	[0,0,1]	[0,0,1]
8		C_{44}		[in xy plane]
9	v	C_{v+}	[0,1,1]	$[0, 2C_{v+} - C_{33} - C_{44}, C_{13} + C_{44} - C_{14}]$
10		C_{v0}		[1,0,0]
11		C_{v-}		$[0, 2C_{v-} - C_{33} - C_{44}, C_{13} + C_{44} - C_{14}]$
13	u	C_{u0}	[0,−1,1]	[1,0,0]
12		C_{u+}		$[0, C_{33} + C_{44} - 2C_{u+}, C_{13} + C_{44} + C_{14}]$
14		C_{u-}		$[0, C_{33} + C_{44} - 2C_{u-}, C_{13} + C_{44} + C_{14}]$

$2C_{x\pm} = (C_{44} + C_{66}) \pm [(C_{44} - C_{66})^2 + 4C_{14}^2]^{1/2}$
$2C_{y\pm} = (C_{11} + C_{44}) \pm [(C_{11} - C_{44})^2 + 4C_{12}^2]^{1/2}$
$2C_{v0} = C_{44} + C_{66} + 2C_{14}$
$4C_{v\pm} = (C_{11} + C_{33} + 2C_{44} - 2C_{14}) \pm [(C_{11} - C_{33} - 2C_{14})^2 + (C_{13} + C_{44} - C_{14})^2]^{1/2}$
$2C_{u0} = C_{44} + C_{66} - 2C_{14}$
$4C_{u\pm} = (C_{11} + C_{33} + 2C_{44} + 2C_{14}) \pm [(C_{11} - C_{33} + 2C_{14})^2 + (C_{13} + C_{44} + C_{14})^2]^{1/2}$

plane and parallel faces cut perpendicular to the wave vector $\vec{k}$. Measurements are performed for a number of directions and polarizations that is sufficient to determine all of the components C_{ij}. Such a set of directions and polarizations is given in Table I, corresponding to those used by Refs. 5 and 6. It is desirable experimentally to use those modes in Table I which are nearly "pure," that is, for which the particle displacement is nearly or exactly perpendicular to $\vec{k}$ (shear) or parallel to $\vec{k}$ (longitudinal). This requirement stems from the availability of commercial quartz transducers to excite these modes.

In an anisotropic medium the direction of the energy flux is not generally the same as the propagation direction.[11] If the angle between these directions is large enough, a portion of the energy in the wave may strike a side face of the sample and be scattered, i.e., suffer "mode conversion." Depending on the sample-transducer geometry, this effect could cause erroneous responses in the measuring apparatus. Of course, unless the direction of energy flux is parallel to $\vec{k}$ by symmetry, its direction cannot be calculated without some knowledge of C_{ij}. In Table II are listed the angle of deviation ϕ_w of the polarization from a pure-mode direction (either parallel or perpendicular to $\vec{k}$), and the angle ϕ_s between the energy flux and the propagation direction. These angles are calculated from the elastic moduli given in the quoted references. Considering the requirement of small ϕ_w and ϕ_s for a successful velocity measurement, the modes numbered 1–3, 7, 9, 10, and 12 are the most promising for Bi_2Te_3. Since these involve propagation along all but the y axis in Table I, it was decided to prepare samples with faces perpendicular to all five directions in the table.

C. cw Resonance Experiment

The cw resonance method[12] was used to perform the velocity measurements. An rf voltage from the tank circuit in the Q meter is impressed across the system of the sample and a quartz piezoelectric transducer bonded to it. The frequency is varied, while maintaining the tank circuit in resonance, until a standing-wave condition in the sample-transducer system is achieved, corresponding to a sharp drop in the Q. The resonance frequency may be read accurately from an electronic counter. As the frequency is varied further, a series of similar resonances is found with nearly equal spacing. The velocity is approximately $2d_s\,\Delta f$, where d_s is the sample dimension parallel to q and Δf is the spacing of resonances.

Corrections for the transducer and bond, amounting to a few percent, must be included in an accurate velocity calculation. By considering the system of the sample, transducer, and bond as a loss-free transmission line, the condition for a resonance may be written

$$Z_s \tan\theta_s + Z_t \tan\theta_t + Z_b \tan\theta_b = (Z_s Z_t / Z_b) \tan\theta_t \tan\theta_s \tan\theta_b \,, \quad (4)$$

where $Z_s = \rho_s v_s$ and $\theta_s = 2\pi f d_s / v_s$ for the sample, with similar expressions for the transducer and bond. For each medium the quantities ρ, d, and v are the density, dimension along $\vec{k}$, and velocity of sound. Grouping terms containing v_s, one obtains the nonlinear equation

$$\tan\theta_s + A\theta_s = 0 \,, \quad (5)$$

in which A is a constant depending on the measured

TABLE II. Angles ϕ_w and ϕ_s (in deg) for propagation in Bi, Sb, and Bi_2Te_3.

Mode number	Effective modulus	Mode description	Bi[a]		Sb[b]		Bi_2Te_3[c]	
			ϕ_w	ϕ_s	ϕ_w	ϕ_s	ϕ_w	ϕ_s
1	C_{11}	long	0	0	0	0	0	0
2	C_{x+}	shear	0	0	0	0	0	0
3	C_{x-}	shear	0	0	0	0	0	0
5	C_{66}	shear	0	20.4	0	32.3	0	29.6
4	C_{y+}	quasilong	7.8	10.4	17.9	20.1	16.4	20.4
6	C_{y-}	quasishear	7.8	24.2	17.9	28.0	16.4	30.2
7	C_{33}	long	0	0	0	0	0	0
8	C_{44}	shear	0	32.5	0	28.7	0	25.8
10	C_{v0}	shear	0	10.2	0	2.6	0	3.0
9	C_{v+}	quasilong	5.3	8.7	3.7	4.3	2.0	2.5
11	C_{v-}	quasishear	5.3	25.6	3.7	44.7	2.0	39.7
13	C_{u0}	shear	0	26.4	0	9.9	0	9.4
12	C_{u+}	quasilong	12.4	17.0	14.6	14.9	9.6	11.0
14	C_{u-}	quasishear	12.4	25.5	14.6	12.6	9.6	24.4

[a]Reference 5. [b]Reference 6. [c]This work.

TABLE III. Description of samples used in this work.

Sample	Faces	Dimension at 20 °C (cm)	Carrier density (cm^{-3})
62AR41	x	0.5425	4×10^{18}
	y	0.6071	
	z	0.3670	
62AR12	x	0.6632	4×10^{18}
	v	0.3152	
	u	0.4877	
63MI	z	0.3327	3.5×10^{19}

frequency of the resonance and known properties of the sample, transducer, and bond. From Eq. (4), this constant can be expressed as

$$A=\frac{1}{2\pi f\rho_s d_s}\left(\frac{Z_t\tan\theta_t+Z_b\tan\theta_b}{1-(Z_t/Z_b)\tan\theta_t\tan\theta_b}\right) . \quad (6)$$

The effective elastic modulus can be found from θ_s using the relation

$$C=\rho_s v_s^2=\rho_s(2\pi f d_s/\theta_s)^2 , \quad (7)$$

so that Eq. (5) yields a value for C for each resonance. Some care must be taken in solving this equation to ensure that the correct branch of the tangent is used; this corresponds to the choice of the correct resonance order, discussed in Ref. 12.

The Bi_2Te_3 samples were prepared from 99.999%-pure elements using a horizontal loaded-zone technique. Single-crystal regions were selected from the resulting ingot and oriented by Laue back-reflection x-ray photographs. The faces were cut by spark erosion and etched lightly in aqua regia. Three specimens, each in the form of a rectangular parallelepiped, were used, their orientation, dimensions (accurate to 0.0005 cm), and carrier concentrations being given in Table III. The faces on sample 62AR41, which were perpendicular to the trigonal axis, were refined by cleaving a thin layer from the surface.

The transducers were X-cut quartz (for longitudinal waves) and Y-cut quartz (for shear waves) in the shape of disks of diameter 0.3175 cm with one plated electrode. At 293 K, the quantities in Eq. (6) relating to the transducers are $f_t=10$ MHz, $\rho_t=2.649$ g/cm^3, with $d_t=0.01974$ cm for shear and $d_t=0.02865$ cm for longitudinal types. It was found that Nonaq stopcock grease was a satisfactory bonding agent over the range 4.2–300 K for both shear and longitudinal waves. At room temperature, bonds made with Salol gave a deeper resonance, implying closer coupling between the transducer and the sample. However, these resonances had much more "structure" and the true resonance frequency was difficult to determine.

For frequencies near the transducer frequency f_t, the correction to C due to transducer effects is about $2\rho_t d_t/\rho_s d_s$. This quantity varies from 2 to 6% for the experimental conditions encountered and the transducer terms in (6) must be retained. The analogous quantity for the bond is much smaller, since d_b is below the 0.0002-in. resolution of the micrometer used to measure the sample dimensions Using $d_b=0.0002$ in., it is found that bond effects are less than 0.08% for f near f_t, so that the effect on C is less than the error due to the measurement of d_s and may be ignored.

The cw resonance measurements were performed over the temperature range 4.2–300 K, using an apparatus in which the sample was held in thermal contact with a copper block and both were encased in an evacuated can immersed in a bath of liquid nitrogen or helium. The sample temperature was varied above the bath temperature by controlling the current to a manganin heater coil wound onto the block. A proportional regulator, sensing the difference between the voltage across the thermometer and a variable reference voltage, was used to maintain the sample temperature to within 0.1 K of the desired value during the process of locating the resonance frequencies. Data were taken at roughly 20-K intervals; the sample temperature was determined over the range 30–300 K by a copper-wire resistance thermometer wound onto the block and using the resistance-vs-temperature table of Dauphinee and Preston-Thomas.[13] Below 30 K a carbon resistor embedded in the block was used in place of the copper-wire thermometer. The thermometers were calibrated at liquid-helium, liquid-nitrogen, and ice points, so that the temperature was accurate to 0.5 K, which is equivalent to an error of less than 0.02% in the elastic modulus.

The moduli were corrected for the temperature variation of the sample density ρ_s and dimension d_s. At 293 K, the linear thermal expansion coefficients α_a and α_c for the basal plane and trigonal axis are, respectively,[4]

$$\alpha_a=12.9 \text{ ppm/K} \quad \text{and} \quad \alpha_c=22.2 \text{ ppm/K},$$

which correspond to a volume thermal expansion coefficient of

$$\beta=2\alpha_a+\alpha_c=48.0 \text{ ppm/K} .$$

The volume coefficient at other temperatures is given approximately by the Grüneisen law

$$\beta=\gamma\rho C_v/BM , \quad (8)$$

where γ is a dimensionless parameter, typically between 1 and 3. Using the heat capacity per gram C_v/M obtained from published specific-heat measurements[14] and the bulk modulus of 3.74×10^{11} dyn/cm^{-2} computed from

$$B = [(C_{11} - C_{66})C_{33} - C_{13}^2]/(C_{11} - C_{66} + C_{33} - 2C_{13}) , \quad (9)$$

one obtains a Grüneisen parameter of 1.49 from Eq. (8). The linear expansion coefficients at other temperatures were calculated from β on the assumption that the ratio α_a/α_c was independent of temperature; a numerical integration then provided the density and sample dimensions as a function of temperature. The lattice parameters at absolute zero obtained from this process are

$$a_0 = 4.3699 \text{ Å}, \quad c_0 = 30.325 \text{ Å} .$$

The results of the cw resonance measurements using propagation modes 1–3, 7–10, and 13 are shown in Figs. 2 and 3. Because of the energy flux dispersion, it was not possible to use the faces cut perpendicular to the y axis. However, by careful positioning of the transducer it was possible to measure C_{44} by mode 8 in spite of the large value of ϕ_s. An additional measurement of mode 2 over the range 80–300 K was made but the response deteriorated below this temperature; these results are also shown. The error bars in the figures represent (i) the uncertainty in the sample length measurement; (ii) scatter in the values of C determined from several resonances and due to such effects as sample inhomogeneities, and surface damage, which are difficult to treat theoretically; and (iii) dependence of C on the resonance order due to bond effects, nonparallel surfaces, and misorientation.

D. Results and Discussion

A least-squares fitting procedure was used to determine the six independent elastic moduli by minimizing the weighted differences between the experimentally determined constants and those calculated from the equations in Table I, using a trial set of moduli. The least-squares procedure does not distinguish between two possible values for the modulus C_{13}, which arise since it occurs only in mode 9 as a squared term. To resolve the ambiguity the lattice stability conditions[15] may be invoked, namely, that the principal minors of the matrix C_{ij} be positive. The equivalent requirements on the six independent moduli are

$$C_{11} > C_{66} > 0, \quad C_{44} > 0, \quad C_{33} > 0, \quad C_{66}C_{44} - C_{14}^2 > 0,$$
$$C_{33}(C_{11} - C_{66}) - C_{13}^2 > 0 , \quad (10)$$

where the last relation is only satisfied by one of the roots for C_{13}. Of course, the other relations are well satisfied by the fitted moduli. In Table IV, the resulting six fitted values are given as a function of temperature, the values of 0 K being extrapolated from data taken at 4.2 K.

Four of the elastic moduli have been measured previously by Ilisavskii[16] at 300 K. His results are $C_{11} = 6.46$, $C_{66} = 2.88$, $C_{33} = 4.73$, and $C_{44} = 2.50$ in units of 10^{11} dyn/cm^2. The agreement with the present work is only fair, with C_{33} alone differing from the results in Table IV by less than the combined quoted errors. Also there is some doubt about his value for C_{66}, since the propagation and polarization directions quoted do not apply to C_{66} but to some combination of modes 2 and 3 for C_{x+} and C_{x-}. Neither of these latter moduli agree with the value Ilisavskii gives for C_{66}.

For crystals in which each atom is at an inversion center and the interatomic forces are purely central in nature, the elastic modulus tensor C_{ijmn} is symmetric in all four indices and the elastic moduli satisfy the Born relations.[15] For media of rhombohedral symmetry, these are

$$3C_{66}/C_{11} = 1, \quad C_{44}/C_{13} = 1. \quad (11)$$

For the elastic moduli in Table IV, these ratios deviate from unity by 2.3 and 1.3%, respectively, at 300 K. However, since the crystal structure does not have the required inversion symmetry at each atomic site, the extent to which relations (10) are obeyed may not be used as an indication of the importance of central forces and should be regarded as fortuitous.

At low enough temperatures, the specific heat per gram atom due to lattice vibrations is given by the Debye law, namely,

$$C_v = \tfrac{12}{5}\pi^4 N_0 k_B (T/\theta_0)^3. \quad (12)$$

The limiting Debye temperature Θ_0 may be obtained from the elastic moduli at absolute zero by averaging the inverse cube of the wave velocities over all modes and directions of propagation. It may be shown that Θ_0 is given by the equation

TABLE IV. Temperature dependence of the elastic moduli. All units are 10^{11} dyn/cm^2. The moduli are believed accurate to 0.25% except C_{13}, which was determined to 0.5%.

Temp. (K)	C_{11}	C_{66}	C_{33}	C_{44}	C_{13}	C_{14}
0	7.436	2.619	5.160	3.135	2.917	1.541
20	7.430	2.617	5.151	3.125	2.921	1.537
40	7.406	2.606	5.132	3.108	2.911	1.527
60	7.371	2.592	5.107	3.083	2.901	1.515
80	7.332	2.570	5.080	3.059	2.875	1.500
100	7.291	2.549	5.052	3.032	2.856	1.484
120	7.249	2.512	5.025	2.998	2.827	1.457
140	7.206	2.494	4.997	2.972	2.812	1.444
160	7.162	2.475	4.978	2.944	2.800	1.429
180	7.117	2.457	4.939	2.914	2.788	1.415
200	7.072	2.437	4.910	2.884	2.777	1.400
220	7.027	2.416	4.882	2.855	2.762	1.385
240	6.982	2.395	4.853	2.826	2.747	1.369
260	6.937	2.734	4.824	2.798	2.733	1.355
280	6.847	2.335	4.768	2.738	2.704	1.325

$$\Theta_0 = (h/k_B)(3n/4V)^{1/3}\rho^{-1/2}I^{-1/3},$$

$$I = \int_0^{\pi/2} \sin\theta\, d\theta \int_{-\pi/6}^{+\pi/6} d\phi \sum_{i=1}^{3} C_i^{-3/2}, \quad (13)$$

where V is the primitive cell volume, ρ is the density, n is the number of atoms in the basis, and the sum extends over the three effective moduli for each direction θ, ϕ. These effective moduli

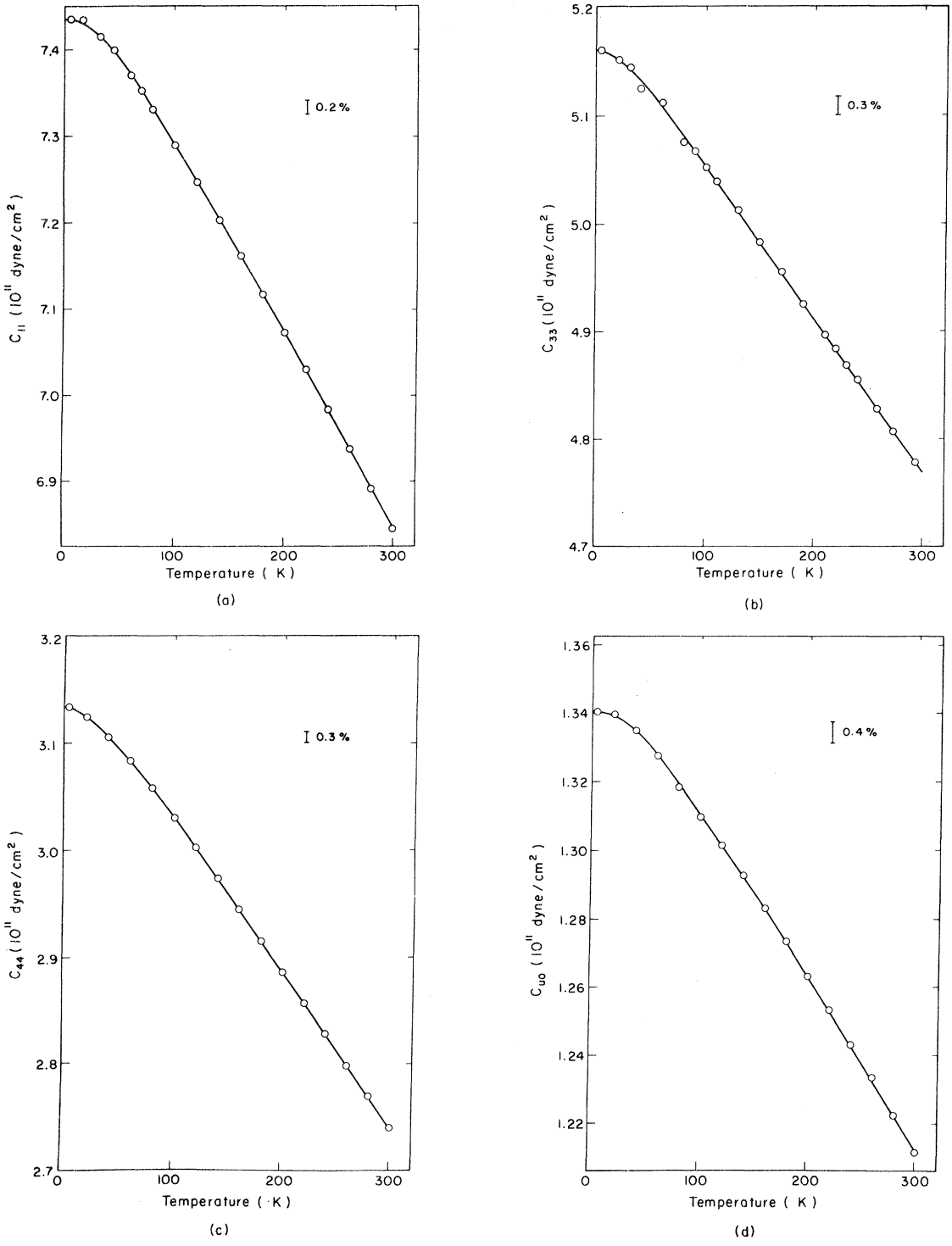

FIG. 2. Temperature variation of the elastic constants (a) C_{11}, (b) C_{33}, (c) C_{44}, and (d) C_{u0} for Bi_2Te_2.

are obtained by solving the secular equation for propagation in a large number of directions and approximating the integral in (13) by a sum, which may be evaluated easily on a computer. The result is $\Theta_0 = 164.9 \pm 0.2$ K, which agrees well with the calorimetric value of the Debye temperature,

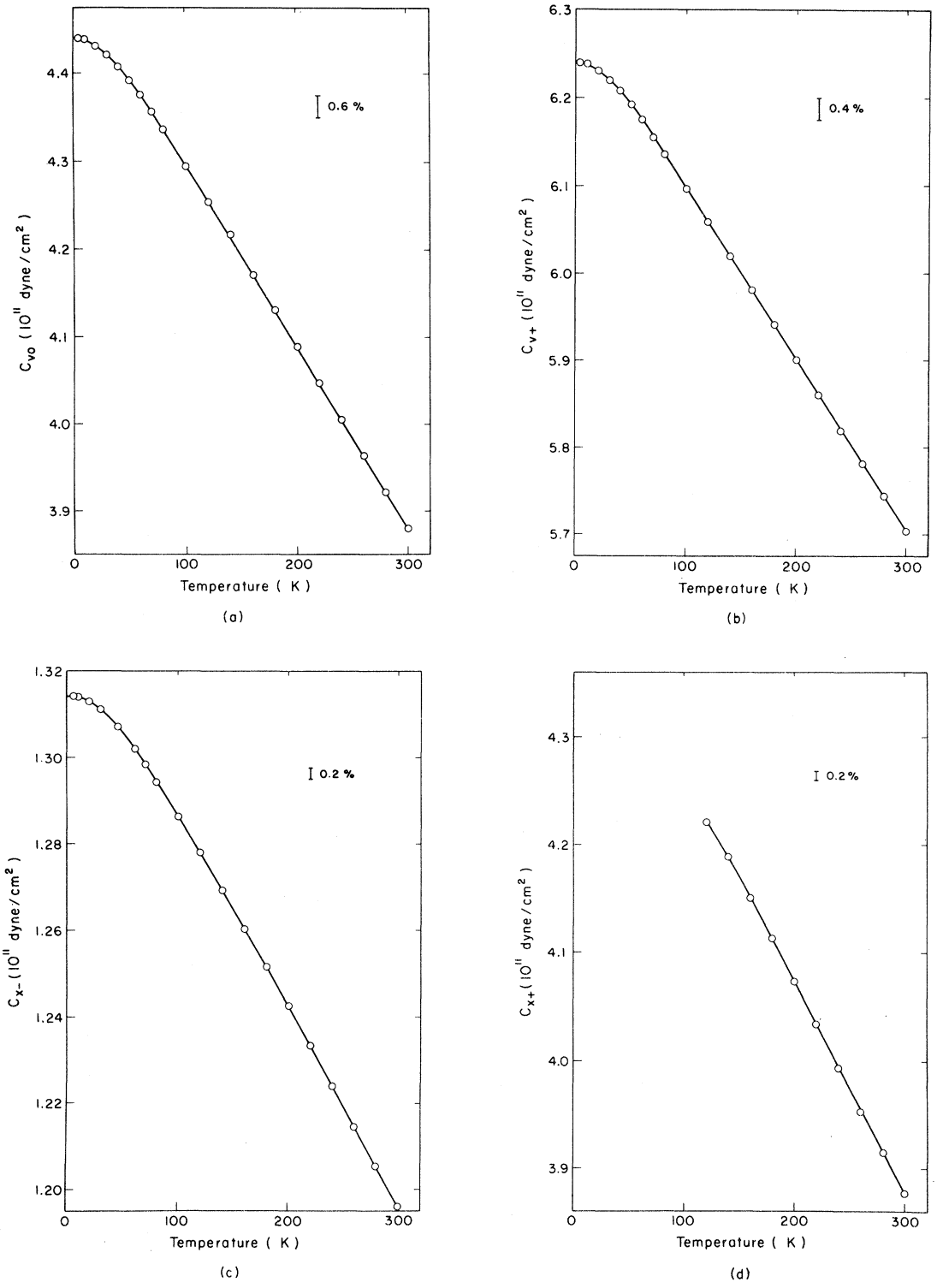

FIG. 3. Temperature variation of the elastic constants (a) C_{v0}, (b) C_{v+}, (c) C_{x-}, and (d) C_{x+} for Bi_2Te_3.

$\Theta_0^{cal} = 165 \pm 2$ K.

III. DETERMINATION OF LATTICE MODEL

In the following sections the Bi_2Te_3 crystal is described in terms of a Born-von Kármán model.[15] Neighboring atoms are assumed to be held together by springlike forces, which may be central or noncentral in character and which are specified by certain adjustable bond parameters. An optimization procedure is used to obtain a best fit of these parameters to the experimentally determined elastic moduli, using the relations between them determined by the model. Once the bond parameters are selected, the dynamical matrix can be diagonalized for a series of $\vec{k}$ values to give the phonon dispersion relations. The density of phonon states and the lattice contribution to the specific heat are found by a root sampling technique and the results are compared with the published specific heat from calorimetric measurements.

A. Force-Constant Matrices

It is assumed that the motion of atoms under acoustic vibration is governed by a crystal potential function Φ. For small atomic displacements $\vec{u}(\vec{l}; s)$ from equilibrium, the potential may be expanded and terms higher than quadratic in $\vec{u}$ discarded, corresponding to the harmonic approximation. In a lattice dynamics calculation, one is interested in the "force-constant" matrix

$$\Phi_{ij}(\vec{l}, \vec{l}'; s, s') = \left(\frac{\partial^2 \Phi}{\partial u_i(\vec{l}; s)\, \partial u_j(\vec{l}'; s')} \right)_0 , \tag{14}$$

which relates the ith component of the force on atom $(\vec{l}; s)$ to the jth component of the displacement of atom $(\vec{l}'; s')$. The total force on atom $(\vec{l}; s)$ is the sum of the contributions from all atoms in the crystal:

$$\vec{f}(\vec{l}; s) = -\sum_{\vec{l}'s'} \vec{\Phi}(\vec{l}, \vec{l}'; s, s') \cdot \vec{u}(\vec{l}'; s') . \tag{15}$$

However, for practical reasons it is assumed that only atoms near to atom $(\vec{l}; s)$ need be considered in (15). For each basis atom there are three neighbors in the next layer above and three neighbors below; these are the first neighbors of the given atom. There are six equivalent atoms in the same layer at a distance a, which are the second neighbors. In this work, only forces between these first and second neighbors, comprising the set of atoms shown in Fig. 1, are considered. The force-constant matrix elements are generally regarded as adjustable parameters to be fitted to elastic moduli, phonon dispersion data, etc. These elements are not all independent but are related to each other by symmetry considerations, which in this case show that there are thirty independent components.

B. Expressions for Elastic Moduli

Born[15] has derived expressions for the elastic moduli in terms of the force-constant matrix elements by considering the propagation of waves in the lattice, and comparing the resulting wave equation with that for a continuum having an elastic modulus tensor C_{ijmn}. The expressions relating the elastic moduli to the thirty force-constant matrix elements of Bi_2Te_3 are rather complicated and will not be presented here.

Since the only measured quantities available to be fitted by the lattice model are the six independent elastic moduli, further assumptions must be made to reduce the number of adjustable parameters. A simple model[17] of the interatomic forces will now be introduced, in which two types of bonds are considered: (a) a central-force bond between two atoms, acting along their line of separation, and (b) an angular-force bond relating three atoms, acting to restore the included angle to its equilibrium value. Only angular bonds, in which the end atoms lie in the same basal plane and the center atom is their first neighbor, will be considered. The strength of each bond is specified by an adjustable bond parameter, dimensionless and of order unity, assigned according to Table V. The 30 independent force-constant matrix elements can then be expressed in terms of the resulting nine bond parameters. Simplifying assumptions, such as that of purely central forces or the absence of second-neighbor interactions, are conveniently introduced by fixing the appropriate bond parameters.

C. Fit of Bond Parameters to Elastic Moduli

It is possible to calculate theoretical values of the six independent elastic moduli from a set of nine bond parameters X_i. Of course, since there are no more than six measured quantities available and hence six independent conditions to be met for a perfect fit, the number of bond parameters per-

TABLE V. Bond parameters used in fitting the lattice model to the elastic moduli of Bi_2Te_3.

Bond parameter	Force type	Bond length or angle	Atoms involved in bond
X_1	central	3.06 Å	Bi-Te_1 in neighboring planes
X_2	central	3.23 Å	Bi-Te_2 in neighboring planes
X_3	central	3.62 Å	Te_1-Te_1 in neighboring planes
X_4	central	4.37 Å	Bi-Bi in same basal plane
X_5	central	4.37 Å	Te_1-Te_1 in same basal plane
X_6	central	4.37 Å	Te_2-Te_2 in same basal plane
X_7	angular	91°	Bi-Te_1-Bi, Te_1-Bi-Te_1
X_8	angular	85°	Bi-Te_2-Bi, Te_2-Bi-Te_2
X_9	angular	74°	Te_1-Te_2-Te_1, Te_2-Te_1-Te_2

TABLE VI. Results of fitting various lattice models to observed elastic moduli.

Model number		1	2	3	4	5
Number of variables		4	5	5	5	6
Relative χ^2		1.1	0.02	0.00003	0.04	0.0
Bond parameters	X_1	29.470	19.728	37.869	26.481	36.155
	X_2	20.516	26.078	16.591	29.341	14.955
	X_3	10.846	9.256	8.612	5.921	9.833
	X_4	1.923	1.818	1.798	2.174	[1.792]
	X_7	[0]	4.829	[0]	[0]	0.782
	X_8	[0]	[0]	3.192	[0]	2.132
	X_9	[0]	[0]	[0]	2.256	0.252
Percent errors in elastic moduli	C_{11}	0.7	−0.5	0.0	0.9	0.0
	C_{66}	−6.4	4.2	0.04	−7.4	0.0
	C_{33}	−14.4	−0.7	−0.03	−0.6	0.0
	C_{44}	−5.0	1.6	0.12	1.6	0.0
	C_{13}	17.6	0.5	0.02	−0.1	0.0
	C_{14}	32.8	−1.2	−0.21	−0.6	0.0

mitted to vary in the fitting procedure must be limited to six or less. Basically the problem is one of minimizing a set of quantities F_i (in this case, the differences between the measured and calculated values of the elastic moduli) as functions of parameters X_i, where the number of functions equals or exceeds the number of parameters. The two methods used[18,19] provide an estimate of the step in parameter space from the current best estimate X_i to the optimum X_i, based on the gradients of the functions F and the history of recent steps. The methods are used iteratively until convergence is obtained.

All combinations of four and five bond parameters consistent with crystal stability, i.e., that provide a force of some kind between each first-neighbor atom pair, were tried. Table VI shows the results for a few of the best fits. The quantity labeled "relative χ^2" is proportional to the sum of the squares of the differences between the measured and calculated moduli and may be taken as an inverse measure of the goodness of the fit. Second-neighbor central-bond parameters X_4, X_5, and X_6 appear in expressions for the elastic moduli only as the sum $B = X_4 + X_5 + 0.5X_6$ and cannot be determined independently by a measurement of the elastic moduli. The quantity shown in Table VI is $X_4 = 0.4B$, which would be obtained if the three parameters were equal. Model 1 includes purely central forces for first and second neighbors. This was the best of the four-parameter models tried, but could only fit C_{14} to 32.8%. Of the five-parameter models tried, only model 3 was able to fit the moduli to experimental accuracy. Models 2 and 4 are included for comparison. In model 5, the quantity X_4 was fixed at 1.792 and X_1, X_2, X_3, X_7, X_8, and X_9 allowed to vary to see the relative magnitudes of X_7, X_8, and X_9 that would be obtained. Of course, in this model the moduli were fitted exactly.

It should be possible to correlate the relative magnitudes of the bond parameters with the proposed chemical bonding schemes.[7,20] The Te_1-Te_1 bond, having parameters X_3 and X_9, is believed to be very nearly of the van der Waals type. Since this force is weak and central, one would expect to find the central bond parameter X_3 smaller than X_1 or X_2 and the angular bond parameter X_9 very small indeed. This is the case in the best fits 1, 3, and 5. It has been suggested that both Bi and Te_2 atoms are bonded covalently with d^2sp^3 orbitals because of their approximately octahedral coordination (note the 85° and 91° angles in Table V), while the shorter Bi-Te_1 bond is supposed to possess an ionic component. On this basis one would expect X_1 and X_2 to be large, with X_1 larger than X_2, while X_7 should be smaller than X_8 because of the central character of the Coulomb interaction, Table VI shows that all models have a large X_1 and X_2, and that the best fits (1, 3, and 5) give X_1 greater than X_2. Also in model 5, where both X_7 and X_8 are allowed to vary, X_7 is less than X_8.

In performing an exact least-squares fit, as in the case of model 5, the parameters obtained are usually quite sensitive to small changes in the functions (experimental C_{ij}) being fitted. Since model 3 was the simplest model able to predict the elastic moduli to experimental accuracy, it was used in all subsequent calculations.

IV. CALCULATIONS USING LATTICE MODEL

A. Dynamical Matrix and Normal Modes

From (13) the equation of motion for the atom $(\vec{t}; s)$ may be written[21]

$$m_s \ddot{u}_i(\vec{t}; s) = -\sum_{\vec{t}' s' j} \Phi_{ij}(\vec{t} - \vec{t}'; s, s') u_j(\vec{t}'; s') , \tag{16}$$

where the sum includes all the matrices consistent with the model discussed above. Introducing the plane-wave solutions

$$u_i(\vec{t}; s) = \frac{1}{(m_s)^{1/2}} w_i(s) e^{2\pi i \vec{k} \cdot \vec{x}(\vec{t}; s) - i\omega t} , \tag{17}$$

the usual determinantal condition is obtained

$$\| D_{ij}(\vec{k}; s, s') - \omega^2 \delta_{ss'} \delta_{ij} \| = 0 , \tag{18}$$

where the dynamical matrix is defined by

$$D_{ij}(\vec{k}; s, s') = \frac{1}{(m_s m_{s'})^{1/2}} \times \sum_{\vec{t}} \Phi_{ij}(\vec{t}; s, s') e^{-2\pi i \vec{k} \cdot \vec{x}(\vec{t}; s, s')} \tag{19}$$

For a given $\vec{k}$ the solution of (18) yields the 15 eigenvalues of the dynamical matrix for Bi_2Te_3,

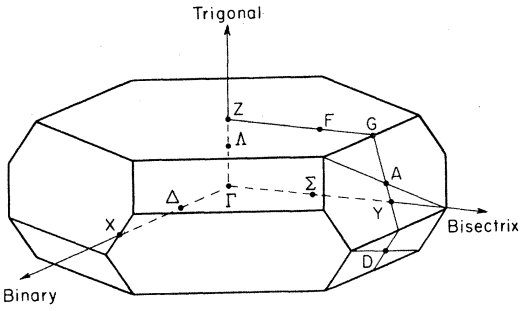

FIG. 4. Brillouin zone for Bi_2Te_3 showing location of principal symmetry points.

which are the normal-mode frequencies. The allowed values of $\vec{k}$ in the plane-wave solutions (17) may be determined by applying the usual periodic boundary conditions. Figure 4 shows the resulting Brillouin zone for Bi_2Te_3 giving the wave vector $\vec{k}$.

By diagonalizing the dynamical matrix determined previously at a series of points along a specific direction in the Brillouin zone, the 15 branches of the dispersion relation $\omega = \omega(\vec{k})$ may be obtained. If the points are taken close enough, it is possible to assign each eigenvalue to its proper branch by making use of the continuity of the branches. Figure 5 shows the dispersion relations for $\vec{k}$ along the trigonal, binary and bisectrix directions. In the limit $\vec{k} \to 0$, three of the eigenvalues approach zero and represent the propagation of acoustic waves in the crystal. The remaining twelve branches are the optical modes and at $\vec{k} = 0$ have the finite values given in Table VII. There are four nondegenerate $\vec{k} = 0$ modes in which the atoms vibrate in the trigonal direction and four doubly degenerate modes in which the atoms vibrate in the basal plane.

B. Group Theory and Optical Activity

The degeneracies found in Table VII may be predicted by a group-theoretical analysis of the $\vec{k} = 0$ modes. At the Brillouin-zone center Γ the group of the wave vector is $\bar{3}m$, the six irreducible representations and their characters being given in Table VIII. The number of acoustic modes at Γ belonging to each irreducible representation is determined by the reduction of the polar-vector representation $A_{1u} + E_u$, while the number of all modes at Γ belonging to each irreducible representation is determined by the reduction of the unit-cell representation $2A_{1g} + 3A_{1u} + 2E_g + 3E_u$. The difference between these two reductions gives the distribution of optical modes among the six irreducible representations. The optical modes in Table VII were assigned to their irreducible representations by an inspection of the eigenvectors.

The selection rules for infrared absorption may be found from the reduction of the polar-vector representation. Thus the optical modes belonging to A_{1u} and E_u are allowed to be infrared active. For infrared photons incident along the trigonal axis, modes 4 and 6 in Table VII may produce reststrahlen at 116.4 and 84.6 cm^{-1}. However, at this time no measurements of optical absorption in this range are available to verify these predictions. The selection rules for Raman scattering are given by the reduction of the second-order symmetric-tensor representation $2A_{1g} + 2E_g$. The components of the electric field and polarizability shown in Table VIII may be found from the basis functions of the representations. Since the group $\bar{3}m$ possesses an inversion center, there is "mutual exclusion" between reststrahlen and Raman scattering, the former occurring for modes belonging to *ungerade* representations and the latter to *gerade* representations.

The degeneracies apparent in Fig. 5 may also be accounted for using group theory. For a general point Λ on the trigonal axis of the Brillouin zone, the group of the wave vector is $3m(C_{3v})$. There are two one-dimensional irreducible representations of this group, A_1 and A_2, and one two-dimensional irreducible representation, E. The unit-cell representation reduces to $5A_1 + 5E$, giving the five nondegenerate and five doubly de-

TABLE VII. Optical modes at Γ.

Mode	ω (10^{12} sec^{-1})	$\bar{\nu}$ (cm^{-1})	Normalized atomic displacements Bi($\bar{2}$)	Te$_1$($\bar{1}$)	Te$_2$(0)	Te$_1$(1)	Bi(2)	Direction	Irr. rep.
1	26.610	141.3	0.359	−0.175	−0.825	−0.175	0.359	z	A_{1u}
2	24.165	128.3	0.310	0.636	0	−0.636	−0.310	z	A_{1g}
3	22.320	118.5	0.346	0.617	0	−0.617	−0.346	x, y	E_g
4	21.923	116.4	0.423	−0.448	−0.491	−0.448	0.423	x, y	E_u
5	17.616	93.5	0.192	−0.574	0.518	−0.574	0.192	z	A_{1u}
6	15.944	84.6	0.012	−0.421	0.803	−0.421	0.012	x, y	E_u
7	13.392	71.1	0.553	−0.441	0	0.441	−0.553	z	A_{1g}
8	9.533	50.6	0.520	−0.479	0	0.479	−0.520	x, y	E_g

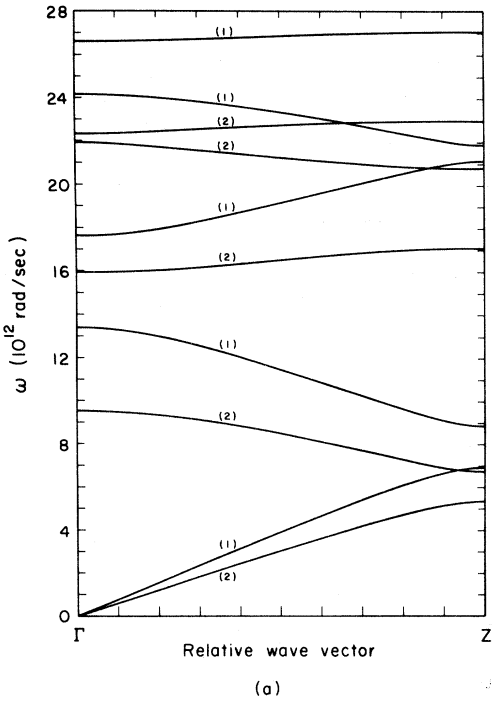

FIG. 5. Calculated phonon dispersion relations for Bi_2Te_3 along principal symmetry directions ΓZ, ΓX, and ΓY. Degeneracies of the modes along the trigonal direction are indicated by the numbers in parentheses.

generate branches shown.

C. Density of States and Specific Heat

In the calculation of the lattice heat capacity of a macroscopic crystal, it is necessary to introduce the distribution function for ω instead of enumerating the frequencies separately. If $g(\omega)d\omega$ is the fraction of frequencies in the interval $(\omega, \omega+d\omega)$, the normalization condition for $g(\omega)$ is

$$\int_0^\infty g(\omega)d\omega = 1 \ . \tag{20}$$

For a crystal having a basis of n atoms, in thermal equilibrium at a temperature T, the heat capacity per mole is

$$C_v = 3nN_0k_B \int_0^\infty \frac{x^2e^x}{(e^x-1)^2}\, g(\omega)d\omega \ , \tag{21}$$

with $x = \hbar\omega/k_BT$.

To perform the integration in (21) for Bi_2Te_3 it is necessary to approximate $g(\omega)$. The simplest method is to sample a large number of points $\vec{k}$ uniformly distributed in the unit cell and to diagonalize the dynamical matrix at each point. The density-of-states function $g(\omega)$ may then be represented by a suitably normalized histogram of the frequencies obtained. To ensure that the sampled points are uniformly distributed in the unit cell, they were chosen to lie on the sublattice obtained by dividing the basis vectors in reciprocal space by 48. Of the 110 592 points so defined in the unit cell, the 9825 unique under the crystal symmetry operations were sampled and the frequencies weighted according to the number of equivalent

TABLE VIII. Symmetry analysis of lattice modes at Γ.

Irr. rep.	Class characters E	$3\sigma_d$	$2C_{3z}$	I	$3C_2$	$2\bar{C}_{3z}$	Number of modes at Γ Ac.	Opt.	Selection rules for optical activity Reststr.	Raman
A_{1g}	1	1	1	1	1	1	0	2	···	$\alpha_{zz}, \alpha_{xx}+\alpha_{yy}$
A_{1u}	1	1	1	−1	−1	−1	1	2	$\vec{E} \parallel \vec{z}$ axis	···
A_{2g}	1	−1	1	1	−1	1	0	0	···	···
A_{2u}	1	−1	1	−1	1	−1	0	0	···	···
E_g	2	0	−1	2	0	−1	0	2	···	$\alpha_{xz}, \alpha_{yz}, \alpha_{xy}, \alpha_{xx}-\alpha_{yy}$
E_u	2	0	−1	−2	0	1	1	2	$\vec{E} \perp \vec{z}$ axis	···
Polar-vector rep.	3	1	0	−3	−1	0				
Unit-cell rep.	15	5	0	−3	−1	0				
Symm.-tensor rep.	6	2	0	6	2	0				

points in the unit cell. A histogram of the eigenfrequencies was formed with 10 800 bins over the range $0 < \omega < 30\times10^{12}$ rad/sec, a condensed version with 300 cells being shown in Fig. 6. It can be seen that the frequency spectrum is separated into two parts by an energy gap at 15×10^{12} rad/sec, where the lower part contains the acoustic modes and the lowest three optical modes and the upper part contains the remaining nine optical modes. A similar division of the frequency spectrum has been found in bismuth at 12.6×10^{12} rad/sec[22] and is apparent in the published dispersion curves.[23]

The specific heat per gram atom is calculated by substituting the histogram representation of $g(\omega)$ into Eq. (21). The corresponding curve of the Debye temperature is shown in Fig. 7, including smoothed calorimetric data for comparison. At temperatures below about 2 K, only the values of $\omega < 1\times10^{12}$ rad/sec contribute appreciably to C_v because of the exponential dependence on ω of the Einstein specific-heat function in the integrand of (21). The corresponding histogram bins have few counts and the calculated C_v values are therefore inaccurate below this temperature. The val-

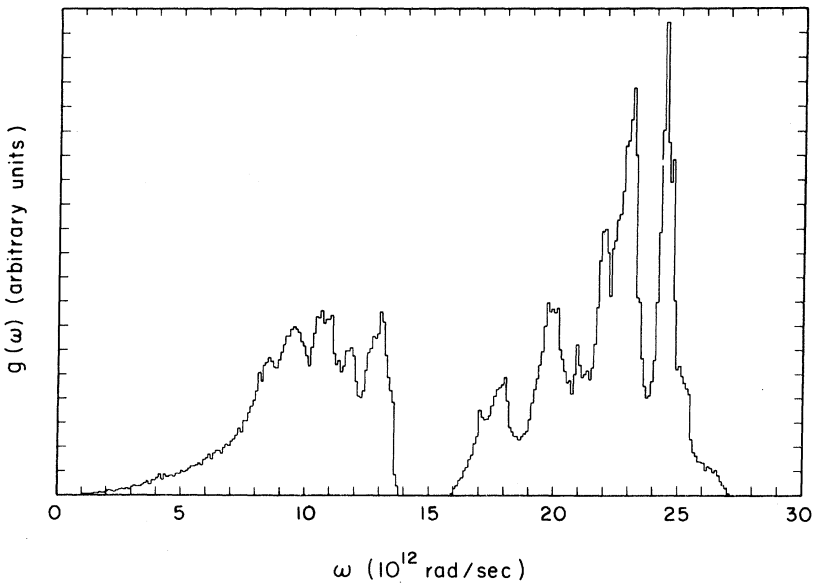

FIG. 6. Calculated density-of-states curve for Bi_2Te_3 with the assumed Born–von Kármán model involving nearest-neighbor and next-nearest-neighbor interactions.

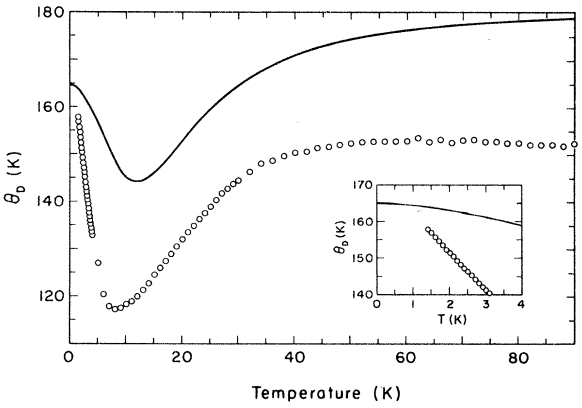

FIG. 7. Comparison of Debye temperature $\Theta_D(T)$ computed from Born–von Kármán model with that obtained calorimetrically.

ue of $\Theta_D(0)$ is known from the elastic moduli, however, and smoothed values of $\Theta_D(T)$ were used below 2 K in Fig. 7.

The true region of validity of the Debye theory appears not to extend above 0.5 K or $\Theta_D/300$, presumably because of a departure from linearity of the acoustic modes for small $\vec{k}$. The discrepancy between the curves at higher temperatures is an indication that a lattice model involving interactions between only first and second neighbors is not an adequate description for Bi_2Te_3. Calculations based on the dispersion curves and elastic moduli of bismuth[3,23] indicate that force contributions from fourth neighbors are significant for this substance. Presumably, the lattice model for Bi_2Te_3 could also be improved by including force contributions from third and fourth neighbors and effects due to the polarizability of the atoms. However, the additional adjustable parameters would make it necessary to acquire more experimental data. The zone-center optical-mode frequencies could be obtained from measurements of infrared absorption or Raman scattering, or points on the dispersion curves could be measured directly by neutron diffraction.

V. CONCLUSIONS

The six independent elastic moduli for Bi_2Te_3 have been determined by a cw resonance experiment over the temperature range 4.2–300 K. The moduli are used to construct a lattice model of the Born–von Kármán type, providing for central and angular forces between first neighbors and central forces between second neighbors. Using the lattice model, the frequencies of infrared absorption and Raman scattering are predicted and the phonon density of states and the lattice specific heat are found. There is a good agreement between the Debye temperature at absolute zero calculated from the elastic moduli and from calorimetric measurements. However, a comparison between the calculated and measured lattice specific heats indicates that the model does not accurately describe the Bi_2Te_3 lattice. Although the general features of the $\Theta_D(T)$ curve are reproduced by the model, the disparity in the $\Theta_D(T)$ values in the temperature range 1–10 K, where only the acoustic modes contribute appreciably to the specific heat, indicates that greater departure from linearity in the dispersion relations of these modes at low $\vec{k}$ is required. Thus is appears that the calculated dispersion curves differ considerably from the true curves for Bi_2Te_3. It has been found that forces from third- and fourth-neighbor atoms are necessary to obtain agreement with the measured dispersion curves in a Born–von Kármán model of the bismuth lattice. If a similar situation exists in the case of Bi_2Te_3, it will be necessary to include third- and fourth-neighbor interactions into the model. It is also possible that first- and second-neighbor forces are sufficient to achieve good agreement in $\Theta_D(T)$, if fewer restrictive assumptions are made about the force-constant matrix elements. In either case the additional degrees of freedom would make it necessary to include more experimental data in the fitting procedure. Thus the next step toward a more sophisticated lattice model should be a determination of the zone-center phonon frequencies by infrared absorption or the Raman effect, or a direct measurement of the phonon dispersion curves by neutron diffraction.

---

†Work supported by a grant from the National Science Foundation. This paper is based on a thesis by one of us (J.J.) as partial fulfillment of the requirements for the Ph.D. degree in Physics at Carnegie-Mellon University.

[1]G. E. Shoemake, J. A. Rayne, and R. W. Ure, Jr., Phys. Rev. 185, 1046 (1969).

[2]H. Ashworth, J. A. Rayne, and R. W. Ure, Jr., Phys. Rev. B 3, 2646 (1971).

[3]D. B. Smith, Ph.D. thesis (University of New Mexico, 1968) (unpublished).

[4]M. H. Francombe, Brit. J. Appl. Phys. 9, 415 (1958).

[5]Y. Eckstein, A. W. Lawson, and D. H. Reneker, J. Appl. Phys. 31, 1534 (1960).

[6]S. Epstein and A. P. de Bretteville, Jr., Phys. Rev. 138, A771 (1965).

[7]J. R. Drabble, in *Progress in Semiconductors*, edited by A. F. Gibson and R. E. Burgess (Wiley, New York, 1963), Vol. 7, p. 45.

[8]J. R. Wiese and L. Muldawer, J. Phys. Chem. Solids 15, 13 (1960).

[9]I. S. Sokolnikoff, *Mathematical Theory of Elasticity*, 2nd ed. (McGraw-Hill, New York, 1956).

[10]H. J. McSkimin, in *Physical Acoustics, Principles and Methods*, edited by W. P. Mason (Academic, New York, 1964), Vol. I A.

[11]M. J. P. Musgrave, *Crystal Acoustics* (Holden-Day, San Francisco, 1970).

[12]D. I. Bolef and M. Menes, J. Appl. Phys. 31, 1010 (1960).

[13]T. M. Dauphinee and H. Preston-Thomas, Rev. Sci. Instr. 25, 884 (1954).

[14]E. S. Itskevich, Zh. Eksperim. i Teor. Fiz. 38, 351 (1960) [Sov. Phys. JETP 11, 255 (1960)].

[15]M. Born and K. Huang, *Dynamical Theory of Crystal Lattices* (Clarendon, Oxford, 1954).

[16]Y. V. Ilisavskii, Fiz. Tverd. Tela 3, 3555 (1961) [Sov. Phys. Solid State 3, 2582 (1962)].

[17]J. de Launay, in *Solid State Physics*, edited by F. Seitz and D. Turnbull (Academic, New York, 1956), Vol. 2, p. 219.

[18]R. Fletcher and M. J. D. Powell, Comput. J. 6, 163 (1963).

[19]N. A. Broste, Ph. D. thesis (Carnegie-Mellon University, 1968) (unpublished).

[20]J. D. Keys and H. P. Dibs, Phys. Status Solidi 19, K11 (1967).

[21]A. A. Maradudin, E. W. Montroll, and G. W. Weiss, in *Solid State Physics*, edited by F. Seitz and D. Turnbull (Academic, New York, 1963), Suppl. 3.

[22]B. A. Kotov, N. M. Okuneva, and E. L. Plachenova, Fiz. Tverd. Tela 11, 2003 (1969) [Sov. Phys. Solid State 11, 1615 (1970)].

[23]J. L. Yarnell, J. L. Warren, R. G. Wenzel, and S. H. Koenig, IBM J. Res. Develop. 8, 234 (1964).